Interface matters: Design of an efficient α-Ag_2WO_4/Ag_3PO_4 photocatalyst

Aline B. Trench[a], *Roman Alvarez*[a], *Vinícius Teodoro*[a], *Thales R. Machado*[a], *Mayara M. Teixeira*[a], *Letícia G. da Trindade*[b], *Daniele Souza*[c], *Ivo M. Pinatti*[d], *Alexandre Z. Simões*[d], *Yara G.* Galvão[c], *Juan Andrés*[e], *Elson Longo*[a].

[a]CDMF – Department of Chemistry, Federal University of São Carlos, 13565-905, São Carlos, SP, Brazil.

[b]Department of Chemistry, São Paulo State University, 17033-360, Bauru, SP, Brazil.

[c]Department of Physics – Federal University of São Carlos, 13565-905, São Carlos, SP, Brazil.

[d]Faculty of Engineering of Guaratinguetá, São Paulo State University (UNESP), 12516-410, Guaratinguetá, SP, Brazil.

[e]Department of Analytical and Physical Chemistry, University Jaume I, 12071, Castellón, Spain.

ABSTRACT

Heterojunction engineering of complex metal oxides is an active area of research that addresses fundamental questions in solid-state systems and have broad technological applications. In this work, α-Ag_2WO_4/Ag_3PO_4 heterojunctions with different amount of α-Ag_2WO_4 (12, 24, and 36 wt%) were synthesized by the coprecipitation method and characterized by X-ray diffraction (XRD), X-ray photoelectron spectroscopy (XPS), field emission scanning electron microscopy (FE-SEM), transmission electron microscopy (TEM), UV-vis diffuse reflectance spectroscopy (UV-DRS), and photoluminescence (PL) emissions. The α-Ag_2WO_4/Ag_3PO_4 heterojunction containing 24% wt of α-Ag_2WO_4 showed the most enhanced photocatalytic activity for the degradation of rhodamine B, which was much higher than Ag_3PO_4 and α-Ag_2WO_4. Trapping experiments reveal that the holes and superoxide radical, in minor extent, were the main active species in the photocatalytic degradation. Such enhanced photocatalytic performance was explained by the surface plasmon resonance effect associated to the presence of metallic Ag at the interface and the formation of a type I heterojunction between α-Ag_2WO_4 and Ag_3PO_4 semiconductors.

Complex oxide heterostructures are an active area of research that addresses fundamental questions in solid-state systems[1–5] and have broad technological applications

.

Keywords: α-Ag_2WO_4/Ag_3PO_4, photocatalytic activity, surface plasmon resonance, type I heterojunction.

INTRODUCTION

Over the past few years, semiconductor photocatalysis has attracted research interest due the synthesis of innovative materials with excellent performance for organic pollutant degradation and waste water cleaning (Li, Zhao et al. 2013, Low, Yu et al. 2017, Byrne, Subramanian et al. 2018). A highly efficient semiconductor need to have a wide range of light absorption, a fast charges separation of photo-generated electron-hole (e^-─h^+) pairs as well as a strong redox ability (Li, Li et al. 2016) (Bocheng Qiu 2017, Wang, Suzuki et al. 2018, Bai, Zhou et al. 2019, Wang, Nakabayashi et al. 2019). However, it is difficult for the single component photocatalyst to possess these characteristics.

To overcome these limitations and improve the performance of a single semiconductor, in the last years two feasible methods have emerged, working via a synergistic interaction/effect: (Mario Bartsch 2017): (i) the formation of heterojunction that involves the combination of two or more semiconductors to form new materials (Lin, Hou et al. 2015, Chen, Yang et al. 2017, Lu, Wang et al. 2017, Rajamohan, Kumaravel et al. 2017, Wang, Hu et al. 2017, Ayappan, Palanivel et al. 2019, Ayappan, Jayaraman et al. 2020, da Silva, Machado et al. 2020, Hezam, Wang et al. 2021), (Wang, Zhang et al. 2014, Zhou, Yu et al. 2014, M. Reza Gholipour 2015). This strategy constitutes a hotspot in recent research (Sudha and Sivakumar 2015, Kar 2017, Low, Yu et al. 2017, Bera, Won et al. 2019, Ge, Zhang et al. 2019) to obtain new materials with superior electrical, optical, and catalytic properties associated to the transfer of the interfacial charge and a synergistic effect between coupled

semiconductors (Kumar, Ojha et al. 2017), and (ii) the deposition of active metal nanoparticles (NPs) (for example, noble metal such as Ag, Au or/and Cu nanoparticles) displaying localized surface plasmon resonance (SPR) effect on the semiconductor´s surface (Hou and Cronin 2013, Ueno and Misawa 2013). In the first case, the photocatalytic activity of heterojunction depends upon the semiconductor type (p or n), chemical composition, and band alignment and location of valence/conduction band potentials. The combination of metal and semiconductor significantly enhances the activity due to two main features: the formation of a Schottky barrier between the metal NPs, resulting in the increased separation efficiency of photogenerated (e^-—h^+) pairs (Bai, Zong et al. 2014). The high electron trapping ability of NPs help to effectively promote the conductivity of NPs, which can then be directly injected into the conduction band of semiconductors (Zheng, Huang et al. 2011), thereby facilitating the charge separation at the interface between NPs and semiconductor, thus improving its photocatalytic ability (Zhou, Liu et al. 2012, Faccin, San-Miguel et al. 2017, Andrés, Gouveia et al. 2018, Assis, Cordoncillo et al. 2018, Li, Liu et al. 2018, Sofi, Majid et al. 2018, da Silva, Faccin et al. 2019, Lemos and Vega 2019, Macedo, Machado et al. 2019, Sofi and Majid 2019, Koyappayil, Berchmans et al. 2020, Nubla and Sandhyarani 2020, Song, Xie et al. 2020, Xia, Min et al. 2021).

The interface drives e^- and h^+ induced in or near this area to move in opposite directions, to promote the charge transfer and suppress the recombination of e^-—h^+ pairs, to increase their stability (Hai Guo 2018), and maximizing the redox power for heterojunction photocatalysts. This is a quantum phenomena in a confined region capable of enhance the simultaneous (successive or parallel) transformation of compounds. As it occurs in other Ag-based semiconductors both Ag_3PO_4 and α-Ag_2WO_4 are unstable and tend to segregate Ag metal nanoparticles (Ag NPs) on the surfaces of these complex oxides. As consequence Ag NPs/Ag_3PO_4 and Ag NPs/α-Ag_2WO_4 composite can be formed, respectively. These composite present SPR effect associated to the ease formation Ag NPs on the surface of these semiconductors (Botelho, Sczancoski et al. 2015, Liu, Huang et al. 2017, Liu, Liu et

al. 2017, Yan, Guan et al. 2017, Andrés, Gouveia et al. 2018, Macedo, Machado et al. 2019, Sofi and Majid 2019, Paulo de Campos da Costa, Assis et al. 2020, Song, Xie et al. 2020).

Despite practical importance and the fact that they were observed for different types of the heterojunction (Linic, Christopher et al. 2011), up to the present there has not been studied a consistent pattern demonstrating the synergy influence of plasmons of Ag NPs on the photocatalytic activity. Inspired by the unique properties of both Ag_3PO_4 and α-Ag_2WO_4, it was envisaged that the coupling of the heterojunction of both materials with presence of Ag NPs at the interface can provide additional active sites, which is anticipated to improve the photocatalytic property significantly. Therefore, in the present work, a first attempt to conduct such studies was done; for that, we purposed to obtain α-Ag_2WO_4/Ag_3PO_4 heterojunction via a facile coprecipitation method. They were taken because their properties could be alternated in a wide range of α-Ag_2WO_4 composition (12, 24, and 36 wt%). The as-synthetized heterojunctions are fully characterized by X-ray diffraction (XRD), X-ray photoelectron spectroscopy (XPS), transmission electron microscopy (TEM), field emission gun scanning electron microscopy (FE-SEM) and diffuse reflectance spectroscopy in the ultraviolet-visible region (UV-vis). This work can also provide important understanding on the role played by the Ag NPs at the interface during the photocatalytic process of the Rhodamine B (RhB) dye degradation. The properties of the photocatalyst were systematically characterized and evaluated and this heterojunction exhibited higher photoactivity than pure counterparts. Furthermore, based on the scavengers result the photocatalytic mechanism is proposed and discussed in detail. Moreover, the stability of the material was studied via recycling and reusability experiments.

RESULTS AND DISCUSSION

The Ag_3PO_4 and α-Ag_2WO_4 were synthesized by the coprecipitation method previously reported(Trench, Machado et al. 2018, Roman Alvarez-Roca 2021). The heterojunctions containing

12, 24, and 36 wt% of α-Ag_2WO_4 in relation to Ag_3PO_4 were synthesized as shown in Figure 1, and were denoted as AWP 1, AWP 2 and AWP 3, respectively.

Figure 1. A synthetic scheme for synthesized AWP 1, AWP 2 and AWP 3 samples.

Figure S1 shows the XRD patterns of the Ag_3PO_4, AWP 1, AWP 2, AWP 3, and α-Ag_2WO_4 samples. The diffraction pattern of Ag_3PO_4 sample are in good agreement with the Inorganic Crystal Structure Database (ICSD) No. 14000 with a cubic structure and a space group $P\bar{4}3n$ (R. Masse 1976). The α-Ag_2WO_4 sample, on the other hand, has an orthorhombic structure with a *Pn2n* space group, according to ICSD No. 4165 (P.M. Skarstad 1975).

It was observed that as the amount of α-Ag_2WO_4 increases, the diffraction peaks referring to this phase are intensified, which is well expected due to the higher content of this material. The presence of XRD patterns related to both phases proves the formation of the heterojunction between Ag_3PO_4 and α-Ag_2WO_4. No characteristics peaks related to any impurities or secondary phase were observed, suggesting that the samples present only α-Ag_2WO_4 and Ag_3PO_4 phases.

TEM analysis was performed for the AWP 2 sample and the Figure 2(a) shows a low-magnified DF-STEM image. It can be noticed two main arrangement of particles in this sample comprising of faceted nanospheres and elongated irregular microparticles covered by these nanospheres. Figure 2(b) displays a magnified view corresponding to the dotted square marked in Figure 2(a). An elemental characterization by EDS was conducted in the microparticle and on the nanospheres, as shown in Figure 2 (b). The resulting EDS spectrum for the microparticle indicates the predominance of Ag, P, W, and O elements, whereas the irregular nanospheres are mainly composed by Ag, P, and O elements. Figure 2 (c-f) shows the EDS mapping of elements Ag, P, W and O corresponding to the region in (b), again confirming the presence of elements referring to the heterojunction and homogeneity of the sample.

To complement this result, a selected area electron diffraction (SAED) analyses (insets) were conducted in the same region of Figure 2 (b) and is shown in Figure 3, as indicated by the dotted arrows, they are shown patterns typically observed in polycrystalline materials. The nanospheres exhibit concentric rings which can be indexed to the (220), (310), and (520) family of planes of cubic Ag_3PO_4, while the patterns on the elongated microparticle reveals the presence of both (402) and (633) family of planes of α-Ag_2WO_4 structure, and (233) family of planes associated to Ag_3PO_4 structure. These results confirm the successful formation of Ag_3PO_4 nanospheres and their crystallization on the surface of α-Ag_2WO_4 microcrystals forming the heterojunction.

Figure 2. TEM characterization of AWP 2 sample: (a) DF-STEM image, (b) high-magnification DF-STEM image and EDS spectra obtained at Ag_3PO_4 crystallized on α-Ag_2WO_4 surface, and (c─f) EDS mapping of Ag, P, W, and O elements corresponding to the region in (b).

Figure 3. DF-STEM image and its corresponding SAED patterns of AWP 2 sample.

Figure 4 shows the micrographs of the pure materials and the heterojunction formed in different proportions. The Ag_3PO_4 structure, represented with orange color, has irregular nanospheres morphology (Figure 4(a)), while the α-Ag_2WO_4 structure, represented with blue color, displays a hexagonal microrod morphology (Figure 4(b)). In the heterojunction (Figure 4(c-e)), it can be seen that the interaction of the materials during the synthesis process provokes changes in the morphology of both materials. As presented in the TEM analysis, the elongated irregular microparticle with blue color is composed of the α-Ag_2WO_4 structure, whereas the smaller nanosphere particles with orange color are the Ag_3PO_4 structure. The change in the morphology of heterojunction are due to dissolution and recrystallization in aqueous medium of the rods to form larger faceted microparticles. The AWP1 sample showed an agglomerate of particles that coalesced to form a large microparticle represented by blue color, which is attributed to the α-Ag_2WO_4 structure, Figure 4(c). The AWP2 and AWP3 samples

showed large microparticles with well-defined surfaces (Figure 4(d-e)). EDS results showed that the α-Ag_2WO_4 microparticles are covered by Ag, P, and O elements, confirming the strong interaction with the smaller nanoparticles that corresponds to the Ag_3PO_4 structure. Moreover, the Ag_3PO_4 nanoparticles present in the heterojunction more defined surfaces.

Figure 4. FE-SEM images of (a) Ag_3PO_4 (orange color), (b) α-Ag_2WO_4 (blue color), (c) AWP 1, (d) AWP 2, and (e) AWP 3.

To investigate the chemical composition and surface structure of the prepared samples, XPS measurements were carried out. The analysis of the high-resolution spectra of constituent elements of α-Ag_2WO_4 and Ag_3PO_4 samples are presented in Figure S2. The deconvolution analysis of P 2*p* spectrum of Ag_3PO_4 as well the W 4*f* spectrum of α-Ag_2WO_4 indicate the presence of P^{5+} and W^{6+} states, as shown in Figure S2(b) and Figure S2(e), respectively (Cai, Zeng et al. 2020, Huang, Li et al. 2020). The deconvolution analysis of Ag 3*d* spectra for both Ag_3PO_4 and α-Ag_2WO_4 samples indicate the presence of Ag^+ and Ag^0 states by their respective spin-orbit coupling peaks, as shown in Figure S2(a) and Figure S2(d), respectively (Hao Zhang 2008, Liu, Fang et al. 2012, Zhang, Yu et al. 2017). Figure S2(c) and Figure S2(f) show the O 1*s* spectra for the Ag_3PO_4 and α-Ag_2WO_4 samples with their components for lattice oxygen (≈ 530 eV), oxygen vacancies (≈ 531.5 eV), and hydroxyl-bounded groups on particle surface (≈ 533 eV), respectively (Sasi and Gopchandran 2007, Yoon, Tak et al. 2014).

The heterojunction with intermediate amount of α-Ag_2WO_4 (AWP 2) was investigated by XPS. The Ag 3*d* spectrum of AWP 2 sample is shown in Figure 5(a), which presented the well-defined components of the spin-orbit coupling related to both Ag^+ and Ag^0 states. The contribution of Ag^0 state arises from the presence of metallic Ag nanoparticles on the surface of Ag_3PO_4 and α-Ag_2WO_4 particles that results in Ag metal/semiconductor interface. The deconvolution analysis of P 2*p* spectrum for AWP 2 sample indicate the presence of P^{5+} state, as shown in Figure 5(b). The O 1*s*

spectrum for the AWP 2 sample with its main components and the survey spectra for Ag_3PO_4, α-Ag_2WO_4, and AWP 2 samples are shown in Figure 5(c) and Figure 5(f), respectively. Variations in the W 4*f* spectrum in the AWP 2 sample in relation to the pure α-Ag_2WO_4 were observed in Figure 5(d), as the broadening of the peaks. The deconvolution results indicated the presented of two oxidation states for W in this sample, the W^{6+} with major proportion and the W^{5+} with minor proportion. The presented components were related to the spin-orbit coupling of W^{6+} $4f_{7/2}$ (35.9 eV) and W^{6+} $4f_{5/2}$ (38.0 eV), W^{5+} $4f_{7/2}$ (35.0 eV) and W^{5+} $4f_{5/2}$ (37.2 eV) (Castillero, Rico-Gavira et al. 2017) and a shoulder related to the W^{6+} loss feature (41.2 eV).

Several works have been reported the effects of heterojunction formation in the surface structure of the materials, such as interfacial strain (Wu, Chen et al. 2019, Jiang, Record et al. 2020, Koohfar, Georgescu et al. 2020, Tian, Zheng et al. 2020). The presence of W^{5+} in the AWP 2 sample can arise from interfacial strain due to lattice mismatch between α-Ag_2WO_4 and Ag_3PO_4, since this latter was grown upon the α-Ag_2WO_4 particles. Furthermore, the W^{6+} reduction can be assigned to the charge transfer effect between α-Ag_2WO_4 and Ag_3PO_4 due to the effective formation of the heterojunction that leads to the energy level alignment (Kung, Li et al. 2019).

Figure 5. High-resolution XPS spectra of (a) Ag 3*d*, (b) P 2*p*, (c) O 1*s* and (d) W 4*f*, (e) content of O 1*s* components of AWP 2 sample and (f) survey of AWP 2, α-Ag_2WO_4 and Ag_3PO_4 samples.

It is well known that the photocatalytic activity of the photocatalysts is closely related to their light absorption ability, thus UV-vis diffuse reflectance spectroscopy is employed to determine the optical absorption properties of the pure Ag_3PO_4, α-Ag_2WO_4, and α-Ag_2WO_4/Ag_3PO_4 heterojunction. The results are represented in Figure 6. The Ag_3PO_4 and α-Ag_2WO_4 samples shows an absorption edge in the visible region at 510 nm and at 405 nm, respectively. It was observed in the heterojunction (AWP 1, AWP 2, and AWP 3) samples that the spectra have two absorption edge wavelengths near of

these absorption edges, proving the presence of the two materials and, therefore the success in the formation of the heterojunction. It was also observed that the absorption edge at 405 nm, referring to α-Ag_2WO_4, had a slight redshift, which favors the use of visible light in the photocatalytic process.

Figure 6. UV–vis diffuses reflectance spectra of Ag_3PO_4, AWP 1, AWP 2, AWP 3, and α-Ag_2WO_4.

The band gap energy (E_g) of the samples α-Ag_2WO_4 and Ag_3PO_4 were presented in Figure S3 by using the Tauc method, equation (1)(Wood and Tauc 1972):

$$(\alpha h\nu)^{2/n} \sim h\nu - E_g \quad (1)$$

where n = 1 for a semiconductor with direct band gap, n = 4 for a semiconductor with indirect band gap, α = absorbance, and $h\nu$ is photon energy. Ag_3PO_4 has an indirect band gap (n = 4) (Botelho, Andres et al. 2016) with an experimental E_g value of 2.40 eV, as shown in figure S3(a). The calculated E_g value is in agreement with those reported in the literature (Ge and Li 2017). Figure S3(b) shows the experimental band gap of α-Ag_2WO_4, which has direct band gap (n = 1) (Nobre, Bastos et al. 2019) with a value of 3.12 eV. This experimental E_g value is also in well agreement with those reported in the literature (Lv, Dai et al. 2017).

Photoluminescence (PL) emission mainly originated from radiative recombination of photo generated electrons and holes (e^-—h^+) trapped in the band tails of semiconductors (Simon, Bouchonville et al. 2014). The higher the emission intensity, the higher the efficiency of charge carrier recombination. (Wang, Ding et al. 2015). Figure 7 exhibits the PL spectra of the as prepared samples under the excitation wavelength of 325 nm and a broad emission peak around 450 nm can be sensed.

. AWP 1 and AWP 2 samples show higher PL intensity than other samples, indicates that both have the highest e^-—h^+ recombination rate that deteriorated the photodegradation efficiency.

An analysis of the results renders that that the PL spectrum of Ag_3PO_4 presents a broadband profile with the maximum emission intensity in the blue region of the visible electromagnetic spectrum at around 454 nm (2.731eV), which is in agreement with the previous results reported in the literature (Botelho, Sczancoski et al. 2015, Tang, Liu et al. 2016). This emission occurs mainly by the charge transfer (e^-─h^+) process between the different clusters that composes the material, such as tetrahedron clusters [PO_4] (Phuruangrat, Ekthammathat et al. 2012, Botelho, Sczancoski et al. 2015, Botelho, Andres et al. 2016). On the other hand, the α-Ag_2WO_4 sample showed a PL intensity peak also in the blue region, centered at 456 nm (2.719eV) and another emission in the red region with a maximum emission intensity between 570 and 650 nm (about 1.984 eV). ESTO NO ES CIERTO The blue emission peak is usually related to distorted octahedron [WO_6] and the emission in the red region can be assigned to the clusters of [AgO_y] with y = 2, 4, 6 and 7, which arises from oxygen vacancies in the semiconductor (Longo, Volanti et al. 2014, Pereira, Santos et al. 2017). The heterojunction samples have also shown emissions in the blue region, at approximately 451 nm, which are close to the blue emission from the isolated materials. Particularly, the AWP 1 and AWP 2 samples showed a similar broadband profile to Ag_3PO_4, while AWP 3 had a similar profile to α-Ag_2WO_4. This result could be associated with the fact that the AWP 3 sample has a higher amount of α-Ag_2WO_4, resulting in a similar band profile of α-Ag_2WO_4. Then, the PL results are consistent to the charge transfer processes of carriers between Ag_3PO_4 and α-Ag_2WO_4 semiconductors in heterojunction.

The AWP 1 and AWP 2 samples showed higher PL intensities at around 454 nm as compared to the other samples which could be associated to a possible increase of charge transfer between both materials. In this way, the e^-─h^+ recombination rate in Ag_3PO_4 decreases, boosting its photocatalytic performance for oxidative reactions, whereas the α-Ag_2WO_4 presented surface defects resulted from the interfacial strain, as a mix of W^{5+} and W^{6+} oxidation states that leads to a higher proportion of distorted [WO_6] clusters in the heterojunction, resulting in a higher emission in the blue region. ESTO HYA QUE REHACERLO

Figure 7. PL spectra of Ag_3PO_4, AWP 1, AWP 2, AWP 3, and α-Ag_2WO_4 samples at 300K.

Photocatalytic activity of the samples

The photocatalytic performance of α-Ag_2WO_4, Ag_3PO_4, and heterojunction AWP 1, AWP 2, and AWP 3 samples were investigated for photodegradation of RhB dye under visible light irradiation. The degradation process was monitored by UV-vis absorption spectra at 554 nm and the degradation curves are shown in Figure 8. It is observed that Ag_3PO_4 has a higher photocatalytic activity compared to α-Ag_2WO_4, degrading approximately 70% of the dye in 10 minutes of reaction, while for α-Ag_2WO_4, no dye degradation was observed in the same reaction time. The use of visible light is the explanation for the low photocatalytic activity of α-Ag_2WO_4 since this material has a band gap energy (Figure S3(a)) that corresponds to excitation in the UV region. Thus, e^- cannot be excited from the valence band (VB) to the conduction band (CB) (Roca, Sczancoski et al. 2015). Ag_3PO_4, on the other hand, has a band gap energy that corresponds to excitation in the visible region, generating the e^-─h^+ pairs under visible light irradiation and consequently degrading the dye, which makes Ag_3PO_4 a promising photocatalyst compared to α-Ag_2WO_4, as it has the possibility of using sunlight irradiation for the degradation of organic compounds. The degradation curves for the heterojunction are also shown in Figure 8, which was noted that all these samples showed a photocatalytic activity superior to that of the isolated materials, demonstrating an effectiveness of the synergistic effect due to formation of heterojunction interface, which promoted a charge carrier transfer, thus improving the photocatalytic activity.

Figure 8. UV–vis absorption spectra of RhB upon photodegradation in the presence of different catalysts.

To investigate the kinetics of the RhB photodegradation reaction, the Langmuir-Hinshelwood model (Rajamohan, Kumaravel et al. 2017) was used, considering a pseudo-first order reaction, according to equation $-\ln (C_N / C_0) = kt$, where C_N and C_0 represent the RhB concentration at different time intervals and in the initial stage, respectively, k and t for the rate constant and irradiation time correspondingly, respectively. Figure 9(a) shows the variations in RhB concentration as C_N/C_0 *versus* irradiation time for the different samples. The photolysis experiment was also performed and shown in Figure 8(a), where it can be seen that there was no degradation. Figure 9(b) shows the values found for the rate constants (k) using the Langmuir-Hinshelwood model mentioned above. It was observed that the heterojunction showed k values higher than those of isolated materials, with the AWP 2 sample showing a value 4.13 times higher than that of Ag_3PO_4 and 458 times higher than α-Ag_2WO_4, being the sample with higher photocatalytic activity.

Note that the value of k increases from the AWP 1 sample with respect to the AWP 2 sample, and it is possible that the greater amount of α-Ag_2WO_4 inserted in the AWP 2 sample increased the synergistic effect between α-Ag_2WO_4 and Ag_3PO_4, to enhanced the transfer of charge carriers and improving the photocatalytic activity of the AWP 2 sample. The value of for the AWP 3 sample decreases in relation to the AWP 2 sample, and a possible explanation to this fact is that AWP 3 sample has the highest amount of α-Ag_2WO_4 in relation to the other heterostructures, thus requiring a higher proportion of UV light for separation of the charge carriers, hampering their photocatalytic activity in comparison with the other heterostructures, but higher than those of isolated materials, since the synergistic effect between the Ag_3PO_4 and α-Ag_2WO_4 samples prevails. In addition, the excess of α-Ag_2WO_4 in the AWP 3 sample causes competition of the active sites for adsorption of species with Ag_3PO_4.

Table 1 shows the photocatalytic efficiency of the α-Ag_2WO_4/Ag_3PO_4 heterojunction synthesized in this work and the comparison with other studies that used Ag_3PO_4 modified or coupled

to another material for RhB photodegradation. The data presented in Table 1 indicate that α-Ag_2WO_4/Ag_3PO_4 heterojunction in this work has a remarkable higher efficiency for the RhB degradation, being the material with the highest rate constant among those reported there. Li. *et al* (Li, Wei et al. 2019) synthesized an α-Ag_2WO_4/Ag_3PO_4 heterostructure for photodegradation of bisphenol A, not mentioning the presence of metallic silver in its heterostructure, thus, it is the first time that the α-Ag_2WO_4/Ag_3PO_4 heterojunction with the presence of Ag NPs is studied for RhB photodegradation under visible light irradiation.

Figure 9. The photodegradation of RhB in the presence of different catalysts and photolysis (a) and degradation rate constants (k) of RhB (b).

Table 1. Comparison of RhB degradation by materials containing Ag_3PO_4 with the reported literature.

To evaluate the stability and reuse of the photocatalyst, recycling experiments were carried out under identical conditions, using the AWP 2 sample, which showed the higher photocatalytic activity. Figure 10 shows 5 cycles carried out for RhB photodegradation, where it can be noted that the first three cycles are relatively stable, with a catalyst deactivation of approximately 27% and 47% only in the fourth and fifth cycles, respectively. This decrease in the photocatalytic activity of the AWP 2 sample may be related to the photocorrosion process that the sample is susceptible, which is well-known phenomenon in Ag-based materials.

Figure 10. Recyclability of the AWP 2 sample for the photocatalytic degradation of RhB under visible light irradiation.

In this study, trapping experiments were performed for the AWP 2 sample to investigate the main reactive species and is shown in Figure 11. The scavenger experiments for $\bullet O_2^-$, $\bullet OH$, and h^+, were investigated by using the capture agents: 1,4-benzoquinone (BQ), t-butyl alcohol (TBA), and ammonium oxalate (AO), respectively (Li, Hu et al. 2017). Meanwhile, RhB degradation process was inhibited by the addition of AO, while when BQ is added, this process was moderately suppressed, i.e. the photocatalytic rate was reduced to 48%. Furthermore, no inhibition is shown by TBA, indicating that $\bullet OH$ does not contribute to the degradation of RhB. These results render that h^+ and $\bullet O_2^-$, in minor extent, are the main active species that participate in the dye degradation ($h^+ > \bullet O_2^- >> \bullet OH$). At this point it is important to note the possible mechanism for the degradation process is very dependent not only of the antioxidant capacity of scavengers, but also to the nature of the radical chain reaction. The chain reactions involving $\bullet O_2^-$ radical participate in the degradation process, as it occurs in the present case, the participation and generation of $\bullet OH$ along the degradation process does not ruled, the scavenging effect of BQ on $\bullet O_2^-$ radical also inhibits the formation of $\bullet OH$ radicals. In this case, the catalytic reaction rate will be greatly reduced by adding either BQ or TBA.

Figure 11. Comparison of photocatalytic degradation of RhB about AWP 2 in the presence of different scavengers under visible light irradiation.

Possible photocatalytic mechanism

It is known that the mechanism for photocatalytic degradation is closely related to the position of conduction band (CB) and valence band (VB) of a semiconductor. As a sequence, to fully understand the photocatalytic reaction mechanism occurring during the photodegradation of the as prepared α-Ag_2WO_4/Ag_3PO_4 heterojunction, the energy band edge positions of the VB and CB of both α-Ag_2WO_4 and Ag_3PO_4 were calculated. The energy band diagram for the heterojunction were

constructed using the equations 2-3, which are based on the Mulliken's electronegativity, *i.e.* the geometric mean of the electronegativity of the constituent atoms in the material composition (Hill notation). (Ray, Dhakal et al. 2018, Sun, Senthil et al. 2018):

$$E_{VB} = \chi - E_e + 0.5E_g \quad (2)$$

$$E_{CB} = E_{VB} - E_g \quad (3)$$

where E_{VB} is the valence band potential, E_{CB} is the conduction band potential, E_e is the free electron energy on the hydrogen scale (~ 4.5 eV), E_g is the semiconductor band gap energy (Figure S3), and χ is the absolute electronegativity (Mulliken's electronegativity) of the semiconductor. For Ag_3PO_4 the value of χ is 5.96 eV (Santos, Martins et al. 2020) and for α-Ag_2WO_4 it is 6.00 eV (Xu, Cao et al. 2018). Thus, employing the equations 2 and 3, the E_{VB} and E_{CB} values of 2.66 eV and 0.26 eV for Ag_3PO_4 and 3.06 eV and -0.06 eV for α-Ag_2WO_4, respectively, were obtained and are in agreement with those reported in the literature (Li, Zhang et al. 2019, Rafiq, Mehraj et al. 2020)

Figure 12 shows two degradation mechanisms proposed for α-Ag_2WO_4/Ag_3PO_4 heterojunction, based on the obtained results. As shown in Figure 12 (a), under visible light irradiation, both Ag_3PO_4 and α-Ag_2WO_4 are excited, generating e^-─h^+ pairs. Due to the energy position of the CB and VB of each material, a type I heterojunction is formed, where the photoexcited e^- in the CB of α-Ag_2WO_4 migrates to the CB of Ag_3PO_4, and the photogenerated h^+ in the VB of α-Ag_2WO_4 also migrates to the VB of Ag_3PO_4, thus generating an accumulation of charge carriers in Ag_3PO_4. These charge carriers perform the reactions to generate the radicals that act on the degradation of RhB dye mainly on the surface of Ag_3PO_4 (da Silva, Machado et al. 2020). In the VB of Ag_3PO_4, both the h^+ that comes from α-Ag_2WO_4 and also the photogenerated h^+ in the Ag_3PO_4 can directly degrade RhB (Sang, Cao et al. 2020, Trench, Machado et al. 2020), as shown in equation 4:

$$h^+ + RhB \rightarrow \text{degradation products} + CO_2 + H_2O \quad (4)$$

The as mentioned reaction is in accordance with the observed scavengers results shown in Figure 11, which indicate that h^+ are the main species acting in the RhB photodegradation.

In CB of Ag_3PO_4, the e^- photoexcited cannot react with dissolved O_2 to produce $\bullet O_2^-$ because its potential (E_{CB} = 0.26 eV vs. NHE) is higher than the potential of $O_2/\bullet O_2^-$ ($E^0(O_2/\bullet O_2^-) = -0.33$ eV vs. NHE) (Rafiq, Mehraj et al. 2020). However, it has been reported that the accumulation of e^- in the surface of Ag_3PO can induce their reaction with adsorbed O_2 to generate $\bullet O_2^-$ (Abroshan, Farhadi et al. 2018, Trench, Machado et al. 2018, Santos, Martins et al. 2020), a specie that acted to a lesser extent on the photodegradation of RhB, as observed in Figure 11, according to equation 5:

$$\bullet O_2^- + RhB \rightarrow \text{degradation products} + CO_2 + H_2O \quad (5)$$

As seen in the scavenger experiments (Figure 11), the $\bullet OH$ species do not participate in the degradation mechanism, and a possible explanation would be that the $\bullet OH$ would be rapidly self-consumed, forming H_2O and O_2 (Trench, Machado et al. 2018), according to the equations 4:

$$4\bullet OH \rightarrow 2H_2O + O_2 \quad (4)$$

As seen in XPS (Figure 5), the Ag NPs formed may be present at the interface of the two semiconductors and could contribute in the separation process of e^-─h^+ pairs due to the surface plasmon resonance (SPR) effect, which creates a cross-linking bridge for the two semiconductors (Hezam, Wang et al. 2021). The surface plasmon excitations are generated under the visible light irradiation and partially converted into energetic electrons on the surface of Ag NPs. Thus, Figure 12 (b) shows a proposed RhB degradation mechanism in the presence of Ag NPs, where it can be seen that the heterojunction remains type I, where the same oxidizing species act. However, e^- photoexcited in α-Ag_2WO_4 can be quickly transferred to Ag NPs. Thus, the e^- that are photoexcited to the CB of α-Ag_2WO_4 are able to migrate to the CB of Ag_3PO_4 more effectively, as they use Ag NPs as a bridge. Therefore, the formation of metallic Ag NPs results in SPR effect, which was advantageous for the effective separation of the charge carriers, resulting in improved photoactivity.

Figure 12. Mechanism of charge carrier transport for α-Ag_2WO_4/Ag_3PO_4 heterojunction photocatalyst

CONCLUSIONS

In conclusion, α-Ag_2WO_4/Ag_3PO_4 heterojunctions with different weight ratios of α-Ag_2WO_4 have been fabricated by a facile chemical precipitation method. Under visible light irradiation, the as-prepared α-Ag_2WO_4/Ag_3PO_4 heterojunction displayed enhanced photocatalytic activity for the photocatalytic degradation of RhB. In particular, the sample with weight content of 12% of (named AWP 2) has showed the highest photocatalytic performance for RhB photodegradation, being degraded of 94.3% in only 5 minutes of exposure to visible light, which is a very promising result when compared with pure materials Ag_3PO_4 and α-Ag_2WO_4, that degrade 45 and 10%, respectively, in the same condition. Our results show that the heterojunction can significantly enhance the absorption of visible light and realize the separation of photogenerated electrons and holes after excitation. Such enhanced photocatalytic performance was explained by the surface plasmon resonance effect associated to the presence of metallic Ag at the interface metallic and the formation of type I heterojunction, which served as a load transfer bridge, avoiding e^--h^+ recombination, which improves the photocatalytic activity of the heterojunction, since charge carriers are available for longer time to react with the adsorbed species.

EXPERIMENTAL

Ag_3PO_4 sample was synthesized by coprecipitation method in aqueous medium at 30 °C. 50 mL of deionized water and the salt $(NH_4)_2HPO_4$ (0.001 mol,) (98.6%, JT Baker) were added to a beaker. This solution was stirred at 30 °C for 10 minutes for a complete dissolution of the salt. In another beaker, the same procedure was performed using 50 mL of deionized water and the $AgNO_3$ salt (0.003 mol) (99.8%, Vetec). After dissolving the salts, the solution containing $AgNO_3$ was added to the $(NH_4)_2HPO_4$ solution and kept under stirring for 10 minutes at 30 °C. Subsequently, the formed precipitate was washed with deionized water to remove residual ions and then dried in an oven at 60 °C for 12 hours.

The α-Ag_2WO_4 crystals were also prepared by coprecipitation method at room temperature, in which $Na_2WO_4 \cdot 2H_2O$ (0.007M) (99.5%, Sigma-Aldrich) and $AgNO_3$ (0.0035M) (99.8 %, Sigma Aldrich) were stirred separately in 50 mL of deionized water at room temperature until the salts dissolve. Subsequently, the $AgNO_3$ solution was added to the Na_2WO_4 solution and stirred for 10 minutes. The formed precipitate was washed with deionized water to remove residual ions and then dried in an oven at 60 °C for 12 hours.

Stoichiometric contents of precursors reagents for α-Ag_2WO_4 and Ag_3PO_4 were used to obtain α-Ag_2WO_4/Ag_3PO_4 heterojunction with 12, 24, and 36 wt% of α-Ag_2WO_4 in relation to Ag_3PO_4, which were denominated as AWP 1, AWP 2, and AWP 3, respectively. For this, α-Ag_2WO_4 was dispersed in a beaker containing 20 mL of deionized water at 30 °C under constant agitation. In another beaker, the $(NH_4)_2HPO_4$ salt was dissolved in 20 mL of deionized water at 30 °C under constant stirring. This solution was added to the beaker containing the dispersed α-Ag_2WO_4 and kept under stirring at 30 °C for 10 minutes. Another solution was prepared using 20 mL of deionized water and $AgNO_3$, which was dissolved under stirring at 30 °C. This solution was dripped onto the suspension containing α-Ag_2WO_4 and $(NH_4)_2HPO_4$ and the whole mixture was stirred for 10 minutes. The precipitate formed was washed with deionized water to remove residual ions and dried in an oven at 60 °C for 12 hours.

Characterization techniques

The obtained materials were characterized by XRD diffraction using a D/Max-2500PC diffractometer (Rigaku, Japan) with CuKα radiation (λ = 1.54056 Å) in the 2θ range of 10° to 80° with a scanning speed of $1^{o}min^{-1}$ and a step size of 0.02°. Transmission electron microscopy (TEM) was performed using a FEI Tecnai G2F20 (Netherlands) microscope operating at 200 kV. Dark field (DF) image as well as local compositional analyzes and mapping via energy-dispersive X-ray spectroscopy (EDS) were recorded in the scanning TEM (STEM) mode. The morphologies of the samples were characterized by using a Field Emission Gun Scanning Electron Microscopy (FE-SEM) in a FEI instrument (Inspection Model F50) operating at 10 kV.

Measurements of X-ray photoelectron spectroscopy (XPS) were performed on a Scientia Omicron ESCA + (Germany) spectrometer using monochromatic Al Kα (1486.7 eV). The maximum deconvolution was performed using a line of 70% Gaussian and 30% Lorentzian with a baseline of the nonlinear Sigmoid type of Shirley. For calibration of the binding energy of the elements, the peak C 1s at 248.8 eV was used as reference. To obtain Ultraviolet-visible (UV-vis) absorption spectra, a Varian Cary 5G (United States) spectrophotometer was used in diffuse reflection mode.

Photoluminescence (PL) measurements were performed by using a 500M SPEX spectrometer coupled with a GaAs-PMT detector. A Kimmon He-Cd laser (325nm line) was used as excitation source. The PL measurements were performed in the range of 380-750 nm with laser power of about 16 mW. All samples were measured at room temperature.

Photocatalytic measurements

The photocatalytic activity of samples of Ag_3PO_4, α-Ag_2WO_4, and heterojunction AWP 1, AWP 2, and AWP 3 were tested for Rhodamine B (RhB) discoloration (95%, Aldrich) under irradiation by visible light. For the photocatalytic experiments, 50 mg of each sample and 50 mL of RhB (10 mg L^{-1}) were used, which were placed in a beaker and later in an ultrasonic bath (Branson, model 1510; frequency 42 kHz) for 15 minutes and then stirred for another 30 minutes, always keeping samples in the dark. An aliquot was collected at time 0 and the RhB solution containing the catalyst was exposed to the irradiation of 6 lamps (Philips TL-D, 15 W). The entire system was maintained at a constant temperature of 20°C. Aliquots were removed at certain times (0, 2, 5, and 10 minutes). All aliquots were centrifuged and their degradation was monitored by measuring the peak of maximum RhB absorption (λ_{max} = 554 nm) using a UV-visible spectrophotometer (V-660, JASCO). A control experiment was carried out under the same conditions, but without the presence of catalysts.

To elucidate the mechanism of α-Ag_2WO_4/Ag_3PO_4 photocatalytic activity enhancement, the main active species which participated in the photocatalytic reaction were investigated. The free

radicals and holes trapping experiments were carried out, in which scavengers experiments were examined by adding of tert-butyl alcohol (TBA, 0,012 mol/L) (Alfa Aesar), ammonium oxalate (AO, 0.012 mol/L) (Alfa Aesar), and benzoquinone (BQ, 0.012 mol/L) (Alfa Aesar), respectively, as scavengers of hydroxyl radical (•OH), hole (h^+), and superoxide radical ($•O_2^-$), respectively.

ACKNOWLEDGMENTS

The authors acknowledge the financial support of the Brazilian research financing institutions: Fundação de Amparo à Pesquisa do Estado de São Paulo (FAPESP, 2013/07296-2, and grant no. 2019/03722-3), Coordenação de Aperfeiçoamento de Pessoal de Nível Superior - Brasil (CAPES) - Finance Code 001 and Conselho Nacional de Desenvolvimento Científico e Tecnológico (CNPq, 142035/2017-3). J.A. acknowledges Universitat Jaume I (project UJI-B2019-30), and the Ministerio de Ciencia, Innovación y Universidades (Spain) (project PGC2018094417-B-I00) for financially supporting this research.

REFERENCES

Abroshan, E., S. Farhadi and A. Zabardasti (2018). "Novel magnetically separable Ag3PO4/MnFe2O4 nanocomposite and its high photocatalytic degradation performance for organic dyes under solar-light irradiation." Solar Energy Materials and Solar Cells **178**: 154-163.

Andrés, J., A. F. Gouveia, L. Gracia, E. Longo, G. Manzeppi Faccin, E. Z. da Silva, D. H. Pereira and M. A. San-Miguel (2018). "Formation of Ag nanoparticles under electron beam irradiation: Atomistic origins from first-principles calculations." International Journal of Quantum Chemistry **118**(9): e25551.

Assis, M., E. Cordoncillo, R. Torres-Mendieta, H. Beltran-Mir, G. Minguez-Vega, R. Oliveira, E. R. Leite, C. C. Foggi, C. E. Vergani, E. Longo and J. Andres (2018). "Towards the scale-up of the formation of nanoparticles on alpha-Ag2WO4 with bactericidal properties by femtosecond laser irradiation." Sci Rep **8**(1): 1884.

Ayappan, C., V. Jayaraman, B. Palanivel, A. Pandikumar and A. Mani (2020). "Facile preparation of novel Sb2S3 nanoparticles/rod-like α-Ag2WO4 heterojunction photocatalysts: Continuous modulation of band structure towards the efficient removal of organic contaminants." Separation and Purification Technology **236**: 116302.

Ayappan, C., B. Palanivel, V. Jayaraman, T. Maiyalagan and A. Mani (2019). "One-step hydrothermal synthesis of CaWO4/α-Ag2WO4 heterojunction: An efficient photocatalyst for removal of organic contaminants." Materials Science in Semiconductor Processing **104**: 104693.
Bai, X., R. Zong, C. Li, D. Liu, Y. Liu and Y. Zhu (2014). "Enhancement of visible photocatalytic activity via Ag@C3N4 core–shell plasmonic composite." Applied Catalysis B: Environmental **147**: 82-91.
Bai, Y., Y. Zhou, J. Zhang, X. Chen, Y. Zhang, J. Liu, J. Wang, F. Wang, C. Chen, C. Li, R. Li and C. Li (2019). "Homophase Junction for Promoting Spatial Charge Separation in Photocatalytic Water Splitting." ACS Catalysis **9**(4): 3242-3252.
Bera, S., D.-I. Won, S. B. Rawal, H. J. Kang and W. I. Lee (2019). "Design of visible-light photocatalysts by coupling of inorganic semiconductors." Catalysis Today **335**: 3-19.
Bocheng Qiu, Q. Z., Mengmeng Du, Linggang Fan, Mingyang Xing, Jinlong Zhang (2017). "Efficient Solar Light Harvesting CdS/Co9S8HollowCubes forZ-SchemePhotocatalytic Water Splitting." Angew. Chem. Int. Ed **56**: 2684 –2688.
Botelho, G., J. Andres, L. Gracia, L. S. Matos and E. Longo (2016). "Photoluminescence and Photocatalytic Properties of Ag3PO4Microcrystals: An Experimental and Theoretical Investigation." ChemPlusChem **81**(2): 202-212.
Botelho, G., J. C. Sczancoski, J. Andres, L. Gracia and E. Longo (2015). "Experimental and Theoretical Study on the Structure, Optical Properties, and Growth of Metallic Silver Nanostructures in Ag3PO4." The Journal of Physical Chemistry C **119**(11): 6293-6306.
Byrne, C., G. Subramanian and S. C. Pillai (2018). "Recent advances in photocatalysis for environmental applications." Journal of Environmental Chemical Engineering **6**(3): 3531-3555.
Cai, T., W. Zeng, Y. Liu, L. Wang, W. Dong, H. Chen and X. Xia (2020). "A promising inorganic-organic Z-scheme photocatalyst Ag3PO4/PDI supermolecule with enhanced photoactivity and photostability for environmental remediation." Applied Catalysis B: Environmental **263**: 118327.
Castillero, P., V. Rico-Gavira, C. López-Santos, A. Barranco, V. Pérez-Dieste, C. Escudero, J. P. Espinós and A. R. González-Elipe (2017). "Formation of Subsurface W5+ Species in Gasochromic Pt/WO3 Thin Films Exposed to Hydrogen." The Journal of Physical Chemistry C **121**(29): 15719-15727.
Chen, F., Q. Yang, X. Li, G. Zeng, D. Wang, C. Niu, J. Zhao, H. An, T. Xie and Y. Deng (2017). "Hierarchical assembly of graphene-bridged Ag3PO4/Ag/BiVO4 (040) Z-scheme photocatalyst: An efficient, sustainable and heterogeneous catalyst with enhanced visible-light photoactivity towards tetracycline degradation under visible light irradiation." Applied Catalysis B: Environmental **200**: 330-342.
da Silva, E. Z., G. M. Faccin, T. R. Machado, N. G. Macedo, M. de Assis, S. Maya-Johnson, J. C. Sczancoski, J. Andrés, E. Longo and M. A. San-Miguel (2019). "Connecting Theory with Experiment to Understand the Sintering Processes of Ag Nanoparticles." The Journal of Physical Chemistry C **123**(17): 11310-11318.
da Silva, J. S., T. R. Machado, A. B. Trench, A. D. Silva, V. Teodoro, P. C. Vieira, T. A. Martins and E. Longo (2020). "Enhanced photocatalytic and antifungal activity of hydroxyapatite/α-AgVO3 composites." Materials Chemistry and Physics **252**: 123294.
Faccin, G. M., M. A. San-Miguel, J. Andres, E. Longo and E. Z. da Silva (2017). "Computational Modeling for the Ag Nanoparticle Coalescence Process: A Case of Surface Plasmon Resonance." The Journal of Physical Chemistry C **121**(12): 7030-7036.
Ge, J., Y. Zhang, Y.-J. Heo and S.-J. Park (2019). "Advanced Design and Synthesis of Composite Photocatalysts for the Remediation of Wastewater: A Review." Catalysts **9**(2): 122.
Ge, M. and Z. Li (2017). "Recent progress in Ag 3 PO 4 -based all-solid-state Z-scheme photocatalytic systems." Chinese Journal of Catalysis **38**(11): 1794-1803.
Hai Guo, C.-G. N., Lei Zhang, Xiao-Ju Wen, Chao Liang, Xue-Gang Zhang, Dan-Lin Guan, Ning Tang, and Guangming Zeng (2018). "Construction of Direct Z-Scheme AgI/Bi2Sn2O7 Nanojunction System with Enhanced Photocatalytic Activity: Accelerated Interfacial Charge Transfer Induced Efficient Cr(VI) Reduction, Tetracycline Degradation and Escherichia coli Inactivation. ." ACS Sustainable Chemistry & Engineering **6**: 8003–8018.
Hao Zhang, G. W., Da Chen, Xiaojun Lv, and Jinghong Li (2008). "Tuning Photoelectrochemical Performances of Ag-TiO_2 Nanocomposites via Reduction/Oxidation of Ag." Chem. Mater. **20**: 6543–6549.

Hezam, A., J. Wang, Q. A. Drmosh, P. Karthik, M. Abdullah Bajiri, K. Namratha, M. Zare, T. R. Lakshmeesha, S. Shivanna, C. Cheng, B. Neppolian and K. Byrappa (2021). "Rational construction of plasmonic Z-scheme Ag-ZnO-CeO2 heterostructures for highly enhanced solar photocatalytic H2 evolution." Applied Surface Science **541**: 148457.
Hou, W. and S. B. Cronin (2013). "A Review of Surface Plasmon Resonance-Enhanced Photocatalysis." Advanced Functional Materials **23**(13): 1612-1619.
Huang, J., D. Li, Y. Liu, R. Li, P. Chen, H. Liu, W. Lv, G. Liu and Y. Feng (2020). "Ultrathin Ag2WO4-coated P-doped g-C3N4 nanosheets with remarkable photocatalytic performance for indomethacin degradation." J Hazard Mater **392**: 122355.
Jiang, P., M.-C. Record and P. Boulet (2020). "First-principles calculations on CuInSe2/AlP heterostructures." Journal of Materials Chemistry C **8**(14): 4732-4742.
Kar, E. K. K. (2017). " Composite Materials Processing, Applications, Characterizations." Springer-Verlag Berlin.
Koohfar, S., A. B. Georgescu, I. Hallsteinsen, R. Sachan, M. A. Roldan, E. Arenholz and D. P. Kumah (2020). "Effect of strain on magnetic and orbital ordering of

LaSrCrO3/LaSrMnO3

heterostructures." Physical Review B **101**(6).
Koyappayil, A., S. Berchmans and M. H. Lee (2020). "Dual enzyme-like properties of silver nanoparticles decorated Ag2WO4 nanorods and its application for H2O2 and glucose sensing." Colloids Surf B Biointerfaces **189**: 110840.
Kumar, S., K. Ojha and A. K. Ganguli (2017). "Interfacial Charge Transfer in Photoelectrochemical Processes." Advanced Materials Interfaces **4**(7): 1600981.
Kung, H. T., P. Li, J. J. Lee, Y. Zhao, A. Dumont and Z. H. Lu (2019). "Reaction and Energy Levels at Oxide–Oxide Heterojunction Interfaces." Advanced Materials Interfaces **6**(22): 1901456.
Lemos, P. S. S., G. S; Roca, R. A; Assis, M.; Torres-Mendieta, R.; Beltrán-Mir, H.; Mínguez- and G. C. Vega, E.; Andrés, J.; and Longo, E. (2019). "Laser and electron beam-induced formation of Ag/Cr structures on Ag2CrO4." Phys. Chem. Chem. Phys. **21**: 6101-6111.
Li, H., Y. Zhang, Q. Zhang, Y. Wang, Y. Fan, X. Gao and J. Niu (2019). "Boosting visible-light photocatalytic degradation of indomethacin by an efficient and photostable Ag3PO4/NG/WO3 composites." Applied Surface Science **490**: 481-491.
Li, J., F. Liu and Y. Li (2018). "Fabrication of an Ag/Ag2MoO4plasmonic photocatalyst with enhanced photocatalytic performance for the degradation of ciprofloxacin." New Journal of Chemistry **42**(14): 12054-12061.
Li, P., X. Zhao, C.-j. Jia, H. Sun, L. Sun, X. Cheng, L. Liu and W. Fan (2013). "ZnWO4/BiOI heterostructures with highly efficient visible light photocatalytic activity: the case of interface lattice and energy level match." Journal of Materials Chemistry A **1**(10): 3421.
Li, S., S. Hu, W. Jiang, Y. Liu, J. Liu and Z. Wang (2017). "Facile synthesis of flower-like Ag3VO4/Bi2WO6 heterojunction with enhanced visible-light photocatalytic activity." J Colloid Interface Sci **501**: 156-163.
Li, T., H. Wei, H. Jia, T. Xia, X. Guo, T. Wang and L. Zhu (2019). "Mechanisms for Highly Efficient Mineralization of Bisphenol A by Heterostructured Ag2WO4/Ag3PO4 under Simulated Solar Light." ACS Sustainable Chemistry & Engineering **7**(4): 4177-4185.
Li, X., J. Li, J. Bai, Y. Dong, L. Li and B. Zhou (2016). "The Inhibition Effect of Tert-Butyl Alcohol on the TiO2 Nano Assays Photoelectrocatalytic Degradation of Different Organics and Its Mechanism." Nanomicro Lett **8**(3): 221-231.
Lin, X., J. Hou, X. Guo, Y. Wang, J. Zheng, C. Liu, Y. Yang and G. Che (2015). "Heterostructured Ag 3 PO 4 /Ag/Bi 3.64 Mo 0.36 O 6.55 nanospheres with enhanced photocatalytic activity under visible light irradiation." Separation and Purification Technology **156**: 875-880.
Linic, S., P. Christopher and D. B. Ingram (2011). "Plasmonic-metal nanostructures for efficient conversion of solar to chemical energy." Nature Materials **10**(12): 911-921.

Liu, D., W. Huang, L. Li, L. Liu, X. Sun, B. Liu, B. Yang and C. Guo (2017). "Experimental and theoretical investigation on photocatalytic activities of 1D Ag/Ag2WO4 nanostructures." Nanotechnology **28**(38): 385702.
Liu, Y., L. Fang, H. Lu, Y. Li, C. Hu and H. Yu (2012). "One-pot pyridine-assisted synthesis of visible-light-driven photocatalyst Ag/Ag3PO4." Applied Catalysis B: Environmental **115-116**: 245-252.
Liu, Z., Y. Liu, P. Xu, Z. Ma, J. Wang and H. Yuan (2017). "Rational Design of Wide Spectral-Responsive Heterostructures of Au Nanorod Coupled Ag3PO4 with Enhanced Photocatalytic Performance." ACS Appl Mater Interfaces **9**(24): 20620-20629.
Longo, E., D. P. Volanti, V. M. Longo, L. Gracia, I. C. Nogueira, M. A. P. Almeida, A. N. Pinheiro, M. M. Ferrer, L. S. Cavalcante and J. Andrés (2014). "Toward an Understanding of the Growth of Ag Filaments on α-Ag2WO4and Their Photoluminescent Properties: A Combined Experimental and Theoretical Study." The Journal of Physical Chemistry C **118**(2): 1229-1239.
Low, J., J. Yu, M. Jaroniec, S. Wageh and A. A. Al-Ghamdi (2017). "Heterojunction Photocatalysts." Adv Mater **29**(20): 1-20.
Lu, J., Y. Wang, F. Liu, L. Zhang and S. Chai (2017). "Fabrication of a direct Z-scheme type WO3/Ag3PO4 composite photocatalyst with enhanced visible-light photocatalytic performances." Applied Surface Science **393**: 180-190.
Lv, J., K. Dai, J. Zhang, L. Lu, C. Liang, L. Geng, Z. Wang, G. Yuan and G. Zhu (2017). "In situ controllable synthesis of novel surface plasmon resonance-enhanced Ag 2 WO 4 /Ag/Bi 2 MoO 6 composite for enhanced and stable visible light photocatalyst." Applied Surface Science **391**: 507-515.
M. Reza Gholipour, T. C. D., F. Béland and T. Do (2015). "Nanocomposite heterojunctions as sunlight-driven photocatalysts for hydrogen production from water splitting." Nanoscale **7**: 8187-8208.
Macedo, N. G., T. R. Machado, R. A. Roca, M. Assis, C. C. Foggi, V. Puerto-Belda, G. Mínguez-Vega, A. Rodrigues, M. A. San-Miguel, E. Cordoncillo, H. Beltrán-Mir, J. Andrés and E. Longo (2019). "Tailoring the Bactericidal Activity of Ag Nanoparticles/α-Ag2WO4 Composite Induced by Electron Beam and Femtosecond Laser Irradiation: Integration of Experiment and Computational Modeling." ACS Applied Bio Materials **2**(2): 824-837.
Mario Bartsch, M. N. (2017). "The Role of Interfaces in Heterostructures." ChemPlusChem 2017 **82**: 42–59.
Nobre, F. X., I. S. Bastos, R. O. Dos Santos Fontenelle, E. A. A. Junior, M. L. Takeno, L. Manzato, J. M. E. de Matos, P. P. Orlandi, J. de Fatima Souza Mendes, W. R. Brito and P. R. da Costa Couceiro (2019). "Antimicrobial properties of alpha-Ag2WO4 rod-like microcrystals synthesized by sonochemistry and sonochemistry followed by hydrothermal conventional method." Ultrason Sonochem **58**: 104620.
Nubla, K. and N. Sandhyarani (2020). "Ag nanoparticles anchored Ag2WO4 nanorods: An efficient methanol tolerant and durable Pt free electro-catalyst toward oxygen reduction reaction." Electrochimica Acta **340**: 135942.
P.M. Skarstad, S. G. (1975). "$(W_4O_{16})^{8-}$ POLYION IN THE HIGH TEMPERATURE MODIFICATION OF SILVER TUNGSTATE." Mat. Res. Bull. **10**: 791-800,.
Paulo de Campos da Costa, J., M. Assis, V. Teodoro, A. Rodrigues, C. Cristina de Foggi, M. A. San-Miguel, J. P. Pereira do Carmo, J. Andrés and E. Longo (2020). "Electron beam irradiation for the formation of thick Ag film on Ag3PO4." RSC Advances **10**(37): 21745-21753.
Pereira, P. F. S., C. C. Santos, A. F. Gouveia, M. M. Ferrer, I. M. Pinatti, G. Botelho, J. R. Sambrano, I. L. V. Rosa, J. Andrés and E. Longo (2017). "α-Ag2–2xZnxWO4 (0 ≤ x ≤ 0.25) Solid Solutions: Structure, Morphology, and Optical Properties." Inorganic Chemistry **56**(13): 7360-7372.
Phuruangrat, A., N. Ekthammathat, S. Thongtem and T. Thongtem (2012). "Preparation of LaPO4 nanowires with high aspect ratio by a facile hydrothermal method and their photoluminescence." Research on Chemical Intermediates **39**(3): 1363-1371.
R. Masse, T., I., Durif, A. (1976). "Refinement of Crystal-Structure of Silver Monophosphate, Ag3PO4-Existence of High-Temperature Form." Zeitschrift Fur Kristallographie **144** 76-81.
Rafiq, U., O. Mehraj, S. Lone, M. Wahid and K. Majid (2020). "Solvothermal synthesis of Ag2WO4/Sb2WO6 heterostructures for enhanced charge transfer properties and efficient visible-light-driven photocatalytic activity and stability." Journal of Environmental Chemical Engineering **8**(5): 104301.

Rajamohan, S., V. Kumaravel, R. Muthuramalingam, S. Ayyadurai, A. Abdel-Wahab, B. Sub Kwak, M. Kang and S. Sreekantan (2017). "Fe3O4–Ag2WO4: facile synthesis, characterization and visible light assisted photocatalytic activity." New Journal of Chemistry **41**(20): 11722-11730.
Ray, S. K., D. Dhakal and S. W. Lee (2018). "Rapid degradation of naproxen by AgBr-α-NiMoO4 composite photocatalyst in visible light: Mechanism and pathways." Chemical Engineering Journal **347**: 836-848.
Roca, R. A., J. C. Sczancoski, I. C. Nogueira, M. T. Fabbro, H. C. Alves, L. Gracia, L. P. S. Santos, C. P. de Sousa, J. Andrés, G. E. Luz, E. Longo and L. S. Cavalcante (2015). "Facet-dependent photocatalytic and antibacterial properties of α-Ag2WO4 crystals: combining experimental data and theoretical insights." Catalysis Science & Technology **5**(8): 4091-4107.
Roman Alvarez-Roca, A. F. G., Camila Cristina de Foggi, Pablo Santana Lemos, Lourdes Gracia, Luís Fernando da Silva, Carlos Eduardo Vergani, Miguel San-Miguel, Elson Longo, and Juan Andrés (2021). "Selective Synthesis of α-, β-, and γ-Ag2WO4 Polymorphs: Promising Platforms for Photocatalytic and Antibacterial Materials." Inorg. Chem **60**: 1062−1079.
Sang, Y., X. Cao, G. Dai, L. Wang, Y. Peng and B. Geng (2020). "Facile one-pot synthesis of novel hierarchical Bi2O3/Bi2S3 nanoflower photocatalyst with intrinsic p-n junction for efficient photocatalytic removals of RhB and Cr(VI)." J Hazard Mater **381**: 120942.
Santos, R. K., T. A. Martins, G. N. Silva, M. V. S. Conceicao, I. C. Nogueira, E. Longo and G. Botelho (2020). "Ag3PO4/NiO Composites with Enhanced Photocatalytic Activity under Visible Light." ACS Omega **5**(34): 21651-21661.
Sasi, B. and K. G. Gopchandran (2007). "Nanostructured mesoporous nickel oxide thin films." Nanotechnology **18**(11): 115613.
Simon, T., N. Bouchonville, M. J. Berr, A. Vaneski, A. Adrovic, D. Volbers, R. Wyrwich, M. Doblinger, A. S. Susha, A. L. Rogach, F. Jackel, J. K. Stolarczyk and J. Feldmann (2014). "Redox shuttle mechanism enhances photocatalytic H2 generation on Ni-decorated CdS nanorods." Nat Mater **13**(11): 1013-1018.
Sofi, F. A. and K. Majid (2019). "Plasmon induced interfacial charge transfer across Zr-based metal-organic framework coupled Ag2WO4 heterojunction functionalized by Ag NPs: Efficient visible light photocatalyst." Chemical Physics Letters **720**: 7-14.
Sofi, F. A., K. Majid and O. Mehraj (2018). "The visible light driven copper based metal-organic-framework heterojunction:HKUST-1@Ag-Ag3PO4 for plasmon enhanced visible light photocatalysis." Journal of Alloys and Compounds **737**: 798-808.
Song, Y., W. Xie, C. Yang, D. Wei, X. Su, L. Li, L. Wang and J. Wang (2020). "Humic acid-assisted synthesis of Ag/Ag2MoO4 and Ag/Ag2WO4 and their highly catalytic reduction of nitro- and azo-aromatics." Journal of Materials Research and Technology **9**(3): 5774-5783.
Sudha, D. and P. Sivakumar (2015). "Review on the photocatalytic activity of various composite catalysts." Chemical Engineering and Processing: Process Intensification **97**: 112-133.
Sun, M., R. Senthil, J. Pan, S. Osman and A. Khan (2018). "A Facile Synthesis of Visible-Light Driven Rod-on-Rod like α-FeOOH/α-AgVO3 Nanocomposite as Greatly Enhanced Photocatalyst for Degradation of Rhodamine B." Catalysts **8**(9): 392.
Tang, C., E. Liu, J. Wan, X. Hu and J. Fan (2016). "Co3O4 nanoparticles decorated Ag3PO4 tetrapods as an efficient visible-light-driven heterojunction photocatalyst." Applied Catalysis B: Environmental **181**: 707-715.
Tian, Y., Q. Zheng and J. Zhao (2020). "Tensile Strain-Controlled Photogenerated Carrier Dynamics at the van der Waals Heterostructure Interface." The Journal of Physical Chemistry Letters **11**(3): 586-590.
Trench, A. B., T. R. Machado, A. F. Gouveia, M. Assis, L. G. da Trindade, C. Santos, A. Perrin, C. Perrin, M. Oliva, J. Andrés and E. Longo (2018). "Connecting structural, optical, and electronic properties and photocatalytic activity of Ag3PO4:Mo complemented by DFT calculations." Applied Catalysis B: Environmental **238**: 198-211.
Trench, A. B., T. R. Machado, A. F. Gouveia, C. C. Foggi, V. Teodoro, I. Sánchez-Montes, M. M. Teixeira, L. G. da Trindade, N. Jacomaci, A. Perrin, C. Perrin, J. M. Aquino, J. Andrés and E. Longo (2020). "Rational Design of W-Doped Ag3PO4 as an Efficient Antibacterial Agent and Photocatalyst for Organic Pollutant Degradation." ACS Omega **5**(37): 23808-23821.

Ueno, K. and H. Misawa (2013). "Surface plasmon-enhanced photochemical reactions." Journal of Photochemistry and Photobiology C: Photochemistry Reviews **15**: 31-52.
Wang, H., L. Zhang, Z. Chen, J. Hu, S. Li, Z. Wang, J. Liu and X. Wang (2014). "Semiconductor heterojunction photocatalysts: design, construction, and photocatalytic performances." Chemical Society Reviews **43**(15): 5234.
Wang, L., J. Ding, Y. Chai, Q. Liu, J. Ren, X. Liu and W. L. Dai (2015). "CeO2 nanorod/g-C3N4/N-rGO composite: enhanced visible-light-driven photocatalytic performance and the role of N-rGO as electronic transfer media." Dalton Trans **44**(24): 11223-11234.
Wang, Q., M. Nakabayashi, T. Hisatomi, S. Sun, S. Akiyama, Z. Wang, Z. Pan, X. Xiao, T. Watanabe, T. Yamada, N. Shibata, T. Takata and K. Domen (2019). "Oxysulfide photocatalyst for visible-light-driven overall water splitting." Nat Mater **18**(8): 827-832.
Wang, Y., H. Suzuki, J. Xie, O. Tomita, D. J. Martin, M. Higashi, D. Kong, R. Abe and J. Tang (2018). "Mimicking Natural Photosynthesis: Solar to Renewable H2 Fuel Synthesis by Z-Scheme Water Splitting Systems." Chem Rev **118**(10): 5201-5241.
Wang, Z., T. Hu, K. Dai, J. Zhang and C. Liang (2017). "Construction of Z-scheme Ag 3 PO 4 /Bi 2 WO 6 composite with excellent visible-light photodegradation activity for removal of organic contaminants." Chinese Journal of Catalysis **38**(12): 2021-2029.
Wood, D. L. and J. Tauc (1972). "Weak Absorption Tails in Amorphous Semiconductors." Physical Review B **5**(8): 3144-3151.
Wu, Z., X. Chen, E. Mu, Y. Liu, Z. Che, C. Dun, F. Sun, X. Wang, Y. Zhang and Z. Hu (2019). "Lattice Strain Enhances Thermoelectric Properties in Sb

2

Te

3

/Te Heterostructure." Advanced Electronic Materials **6**(1): 1900735.
Xia, Z., J. Min, S. Zhou, H. Ma, B. Zhang and X. Tang (2021). "Photocatalytic performance and antibacterial mechanism of Cu/Ag-molybdate powder material." Ceramics International.
Xu, H., Y. Cao, J. Xie, J. Hu, Y. Li and D. Jia (2018). "A construction of Ag-modified raspberry-like AgCl/Ag2WO4 with excellent visible-light photocatalytic property and stability." Materials Research Bulletin **102**: 342-352.
Yan, T., W. Guan, Y. Xiao, J. Tian, Z. Qiao, H. Zhai, W. Li and J. You (2017). "Effect of thermal annealing on the microstructures and photocatalytic performance of silver orthophosphate: The synergistic mechanism of Ag vacancies and metallic Ag." Applied Surface Science **391**: 592-600.
Yoon, D. H., Y. J. Tak, S. P. Park, J. Jung, H. Lee and H. J. Kim (2014). "Simultaneous engineering of the interface and bulk layer of Al/sol-NiOx/Si structured resistive random access memory devices." J. Mater. Chem. C **2**(30): 6148-6154.
Zhang, C., K. Yu, Y. Feng, Y. Chang, T. Yang, Y. Xuan, D. Lei, L.-L. Lou and S. Liu (2017). "Novel 3DOM-SrTiO 3 /Ag/Ag 3 PO 4 ternary Z-scheme photocatalysts with remarkably improved activity and durability for contaminant degradation." Applied Catalysis B: Environmental **210**: 77-87.
Zheng, Z., B. Huang, X. Qin, X. Zhang, Y. Dai and M.-H. Whangbo (2011). "Facile in situ synthesis of visible-light plasmonic photocatalysts M@TiO2 (M = Au, Pt, Ag) and evaluation of their photocatalytic oxidation of benzene to phenol." Journal of Materials Chemistry **21**(25): 9079.
Zhou, P., J. Yu and M. Jaroniec (2014). "All-Solid-State Z-Scheme Photocatalytic Systems." Advanced Materials **26**(29): 4920-4935.
Zhou, X., G. Liu, J. Yu and W. Fan (2012). "Surface plasmon resonance-mediated photocatalysis by noble metal-based composites under visible light." Journal of Materials Chemistry **22**(40): 21337.

Interface matters: Design of an efficient α-Ag_2WO_4/Ag_3PO_4 photocatalyst

Aline B. Trench[a], *Roman Alvarez*[a], *Vinícius Teodoro*[a], *Thales R. Machado*[a], *Mayara M. Teixeira*[a], *Letícia G. da Trindade*[b], *Daniele Souza*[c], *Ivo M. Pinatti*[d], *Alexandre Z. Simões*[d], *Yara G.* Galvão[c], *Juan Andrés*[e], *Elson Longo*[a].

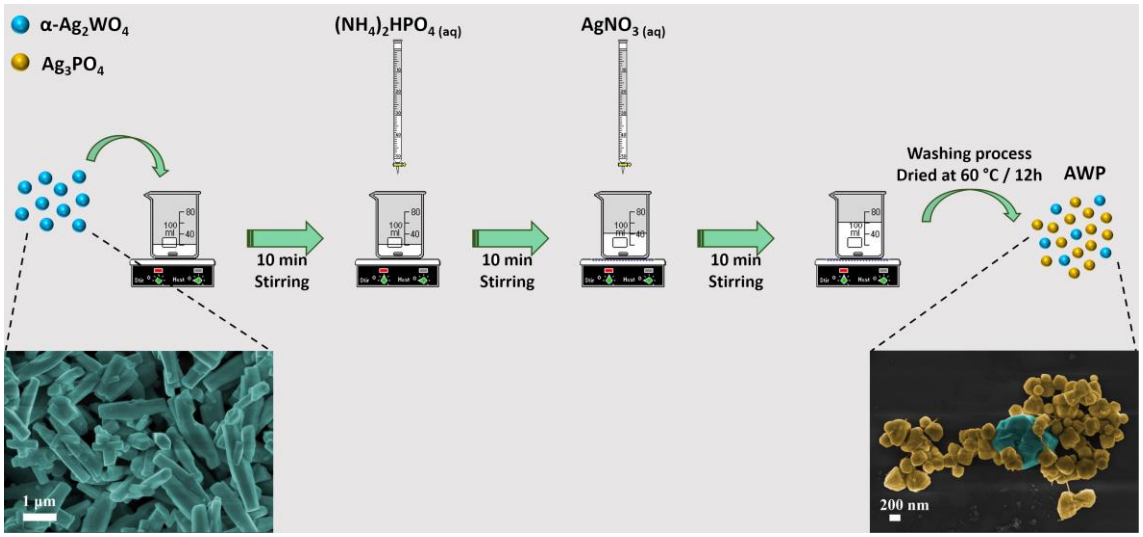

Figure 1. A synthetic scheme for synthesized AWP 1, AWP 2 and AWP 3 samples.

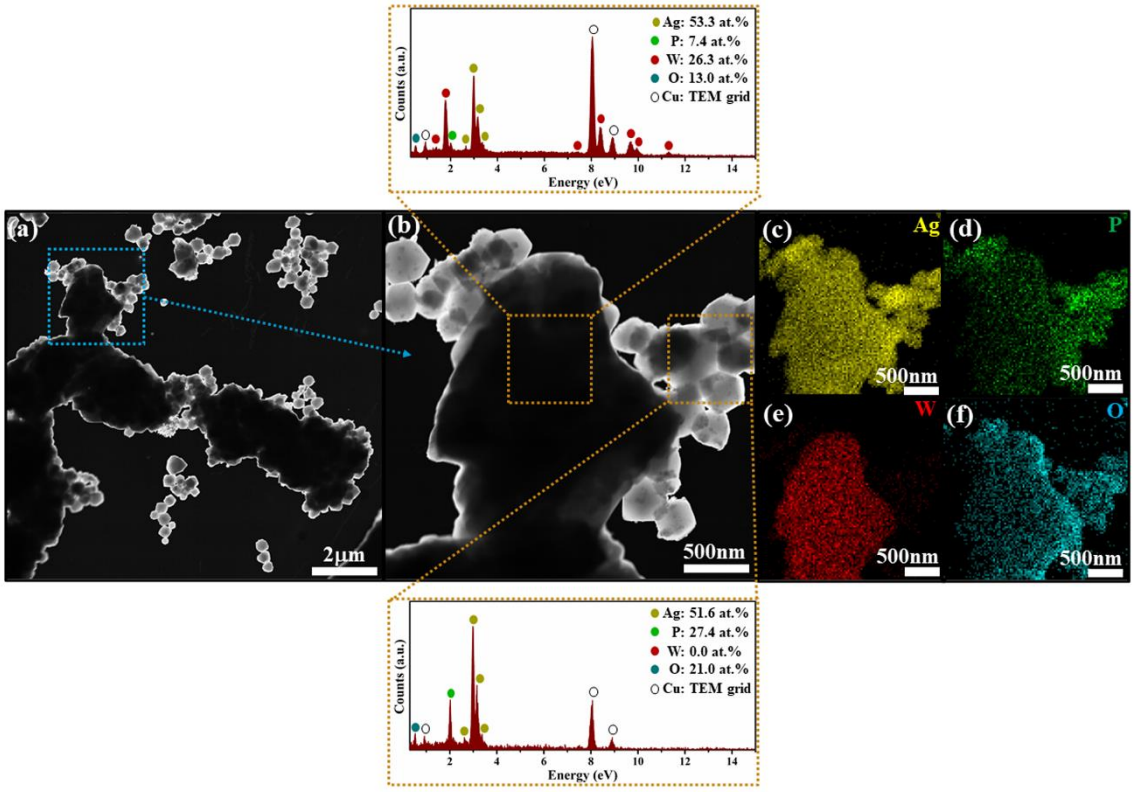

Figure 2. TEM characterization of AWP 2 sample: (a) DF-STEM image, (b) high-magnification DF-STEM image and EDS spectra obtained at Ag_3PO_4 crystallized on α-Ag_2WO_4 surface, and (c─f) EDS mapping of Ag, P, W, and O elements corresponding to the region in (b).

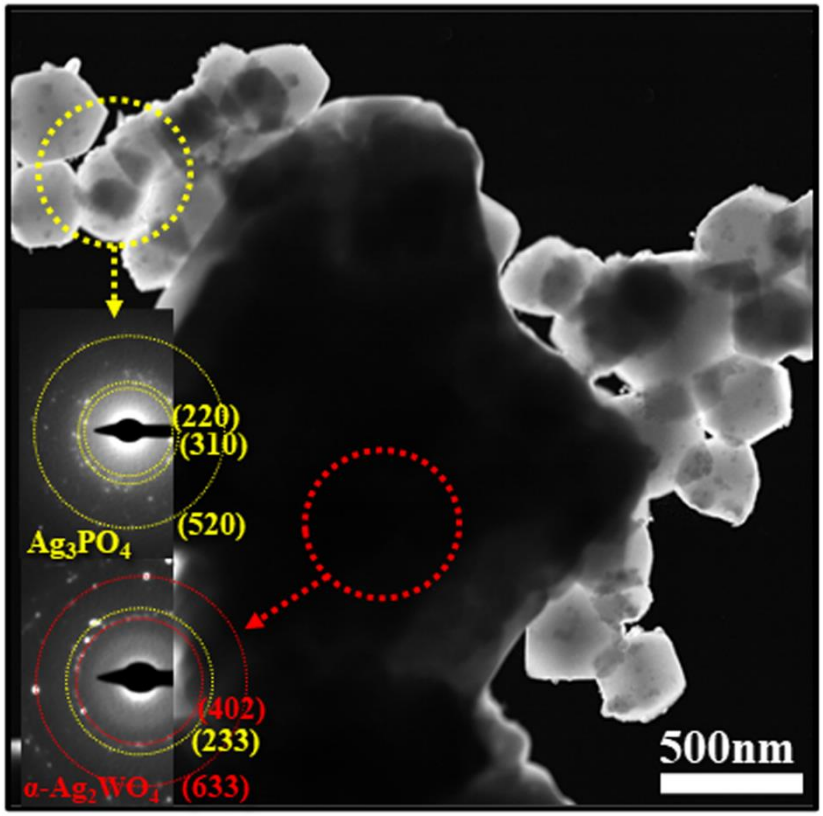

Figure 3. DF-STEM image and its corresponding SAED patterns of AWP 2 sample.

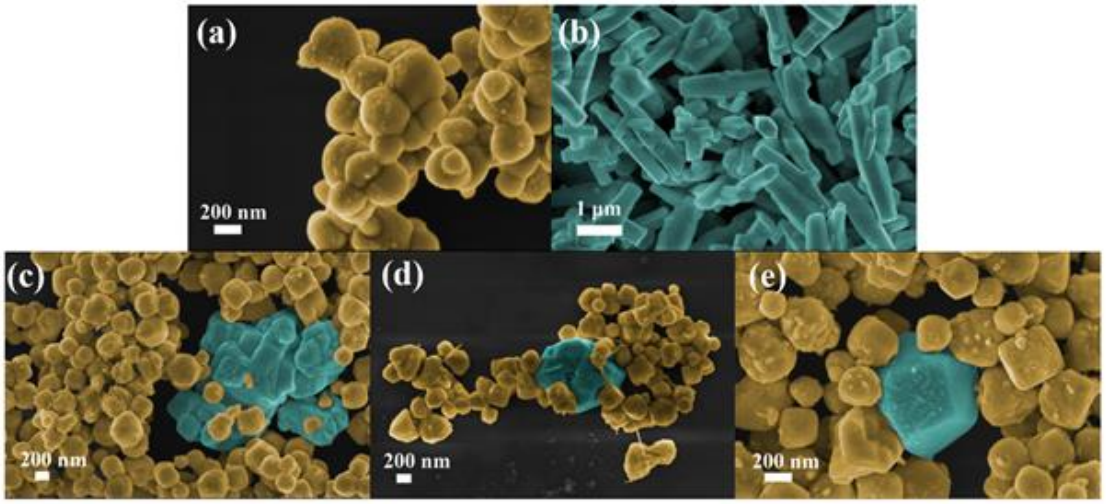

Figure 4. FE-SEM images of (a) Ag_3PO_4 (orange color), (b) α-Ag_2WO_4 (blue color), (c) AWP 1, (d) AWP 2, and (e) AWP 3.

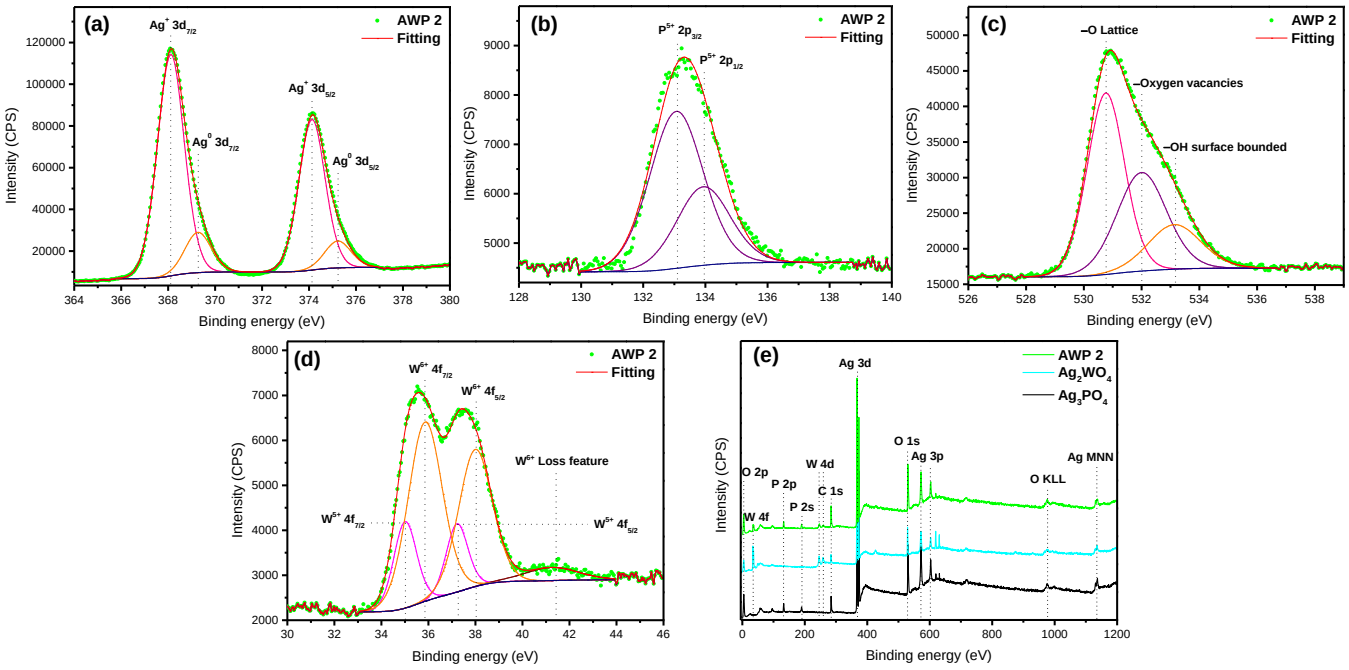

Figure 5. High-resolution XPS spectra of (a) Ag 3*d*, (b) P 2*p*, (c) O 1*s* and (d) W 4*f*, (e) content of O 1*s* components of AWP 2 sample and (f) survey of AWP 2, α-Ag_2WO_4 and Ag_3PO_4 samples.

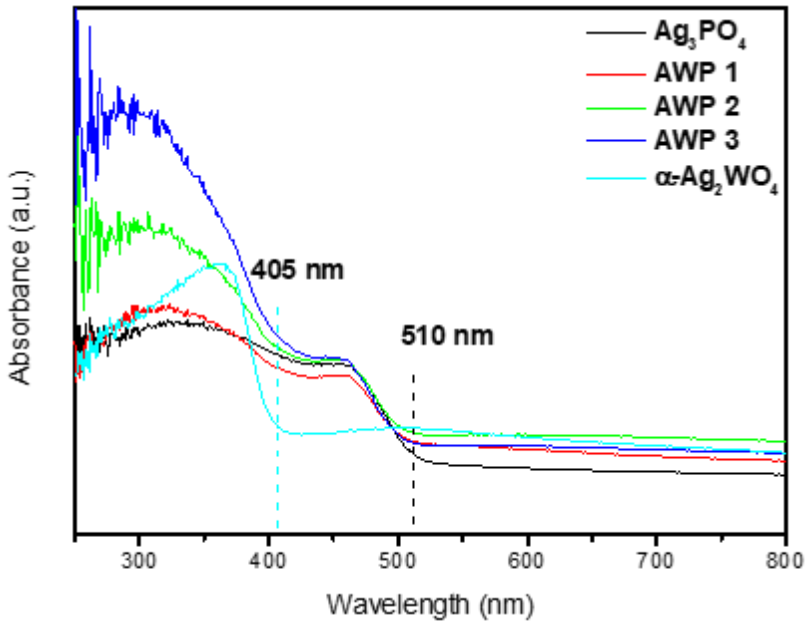

Figure 6. UV–vis diffuses reflectance spectra of Ag_3PO_4, AWP 1, AWP 2, AWP 3, and α-Ag_2WO_4.

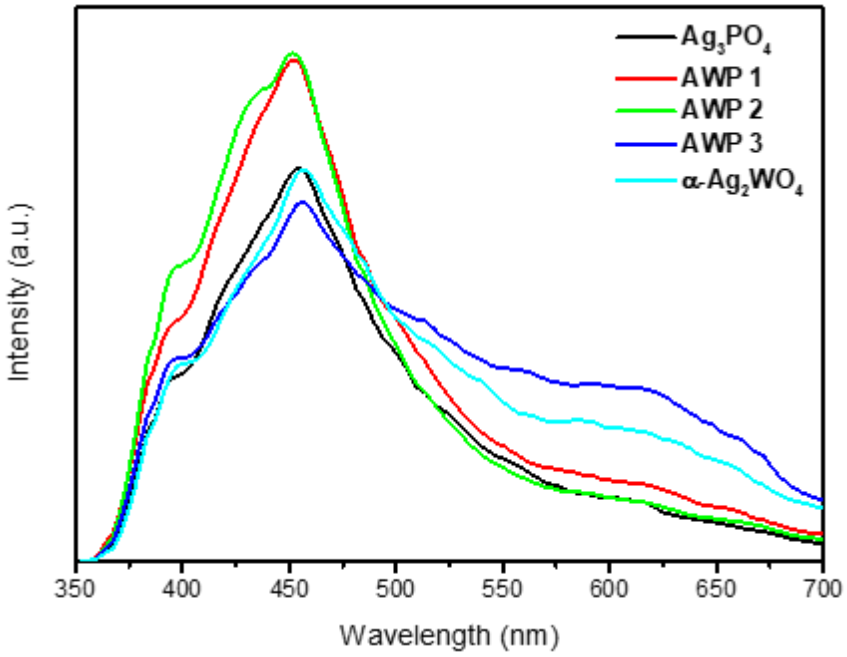

Figure 7. PL spectra of Ag_3PO_4, AWP 1, AWP 2, AWP 3, and α-Ag_2WO_4 samples at 300K.

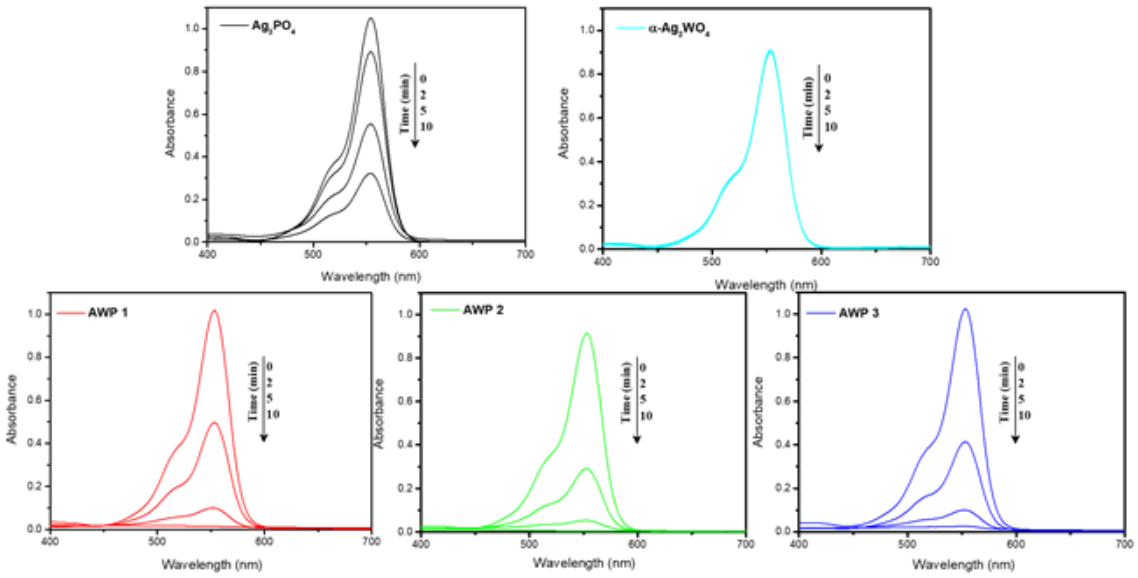

Figure 8. UV–vis absorption spectra of RhB upon photodegradation in the presence of different catalysts.

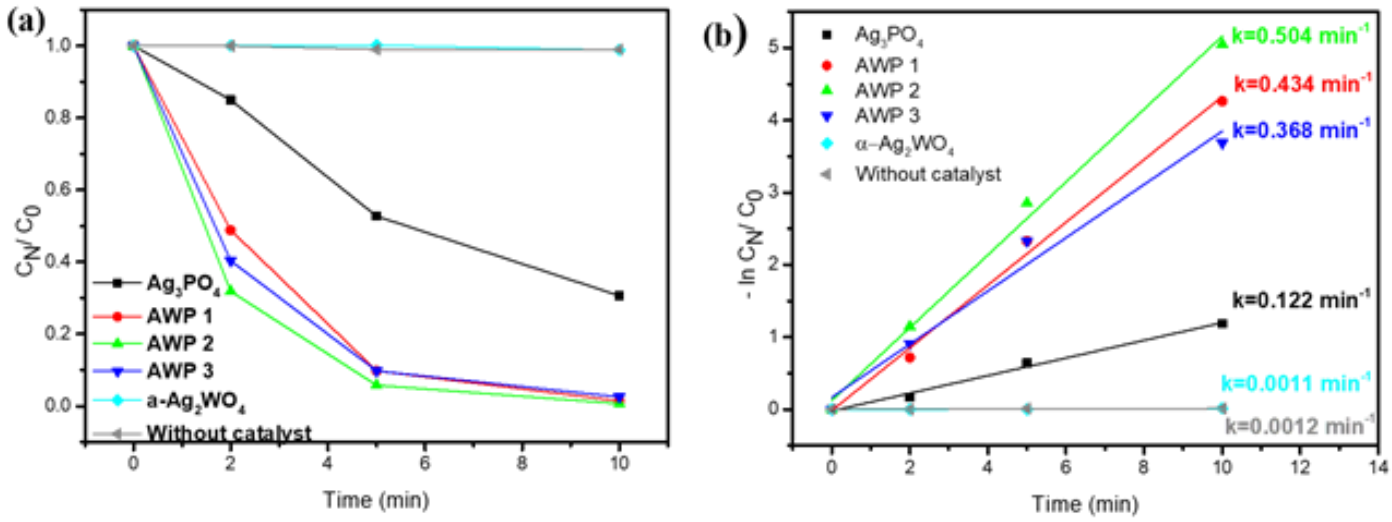

Figure 9. The photodegradation of RhB in the presence of different catalysts and photolysis (a) and degradation rate constants (k) of RhB (b).

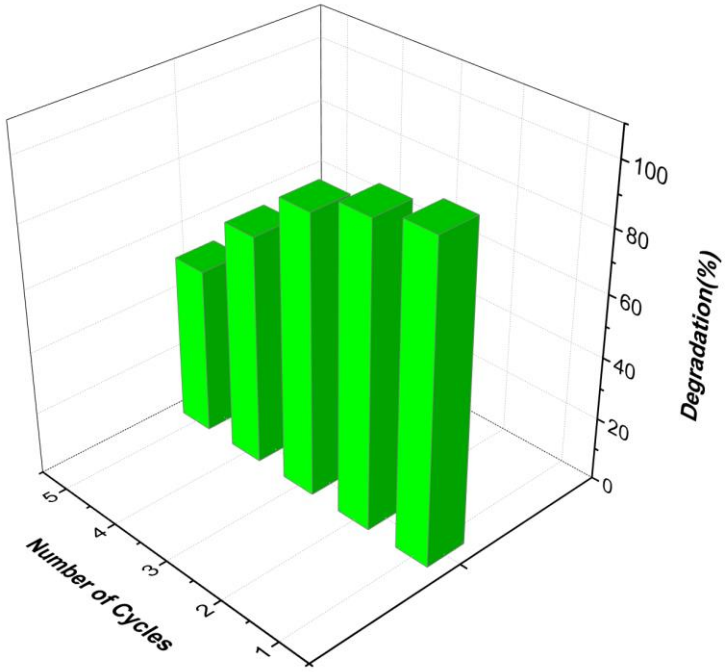

Figure 10. Recyclability of the AWP 2 sample for the photocatalytic degradation of RhB under visible light irradiation.

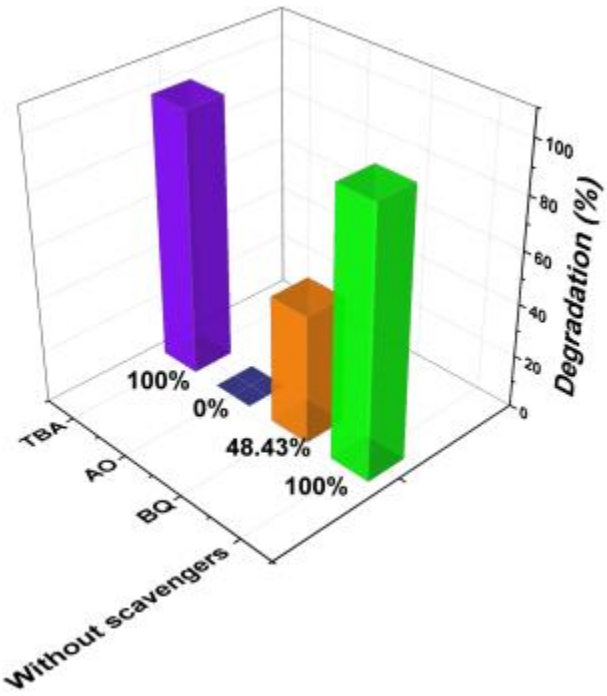

Figure 11. Comparison of photocatalytic degradation of RhB about AWP 2 in the presence of different scavengers under visible light irradiation.

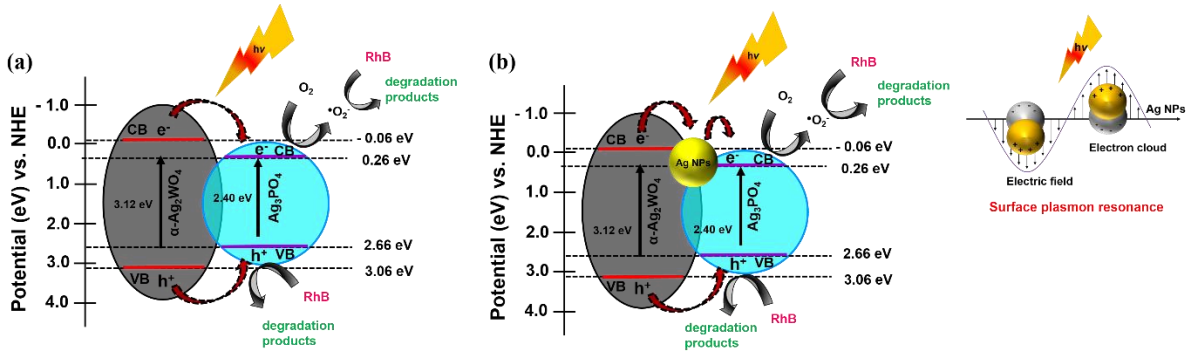

Figure 12. Mechanism of charge carrier transport for α-Ag_2WO_4/Ag_3PO_4 heterojunction photocatalyst

Table 1. Comparison of RhB degradation by materials containing Ag_3PO_4 with the reported literature.

Catalyst	Mass of catalyst (mg)	RhB concentration (mg/L)	Light source	Rate constant (min^{-1})	Time degradation (min)	Reference
Ag_3PO_4/N-TiO_2	20	10	Visible light	0.0194	120	(Khalid, Mazia et al. 2020)
g-C_3N_4@Ag@ Ag_3PO_4	6	20	Visible light	0.030	60	(Li, Wan et al. 2017)
Ag_2MoO_4 /Ag_3PO_4	50	10	Visible light	0.3591	12	(Cao, An et al. 2017)
Ag_3PO_4/NiO	30	5	Visible light	0.2238	30	(Santos, Martins et al. 2020)
Ag_3PO_4/$BiNbO_4$	15	20	Visible light	0.1459	30	(Li, Miao et al. 2019)
Ag_3PO_4@$MgFe_2O_4$	20	10	Visible light	0.1370	30	(Zhou, Zhang et al. 2018)
Ag_3PO_4:Mo	50	10	Visible light	0.347	15	(Trench, Machado et al. 2018)
Ag_3PO_4:W	50	10	Visible light	0.449	10	(Trench, Machado et al. 2020)
α-Ag_2WO_4/Ag_3PO_4	50	10	Visible light	0.504	10	Our work